Insights on the Small Tsunami from 28 January 2020 Caribbean Sea M_W7.7 Earthquake by Numerical Simulation and Spectral Analysis

Zhiguo Xu (xuzhg04@sina.com)
National Marine Environmental Forecasting Center https://orcid.org/0000-0002-3703-7726
Lining Sun
National Marine Environmental Forecasting Center
Mohd Nashriq Abd Rahman
Malaysian Meteorological Department
Shanshan Liang
China Earthquake Networks Center
Jianyu Shi
National Marine Environmental Forecasting Center
Hongwei Li
National Marine Environmental Forecasting Center

Research Article

Keywords: 2020 Caribbean Sea earthquake, strike-slip fault, tsunami, numerical simulation, spectral analysis, submarine landslide

Posted Date: June 14th, 2021

DOI: https://doi.org/10.21203/rs.3.rs-608879/v1

Version of Record: A version of this preprint was published at Natural Hazards on January 15th, 2022.
See the published version at https://doi.org/10.1007/s11069-021-05154-1.

Abstract

A huge left-lateral strike-slip *M*w7.7 earthquake struck the Caribbean Sea on January 28, 2020. Thus, a small tsunami was generated as as result of the earthquake. The information and observational data gathered for the earthquake and tsunami, as well as integrating the regional tectonic setting, were used to describe the seismogenic source's properties. The COMCOT model was used for tsunami simulation, with Okada's dislocation model from finite fault solutions for M_W7.7 Caribbean Sea earthquake published by the USGS. The simulation results were compare to tide gauge records to validate whether the seafloor vertical displacements generated by strike-slip fault caused a small tsunami. We conduct spectral analysis of tsunami to better understand the characteristics of tsunami records. Tsunami simulation results show that the coseismic vertical displacement caused by a strike-slip M_W7.7 earthquake can contribute to the small tsunami, and the anomalously large high-frequency tsunami waves recorded by the George tide gauge in 11 minutes after the earthquake were unrelated to the earthquake-generated tsunami. According to spectrum analysis. The predominant period of the noticeable high frequency tsunami wave recorded by George tide gauge is only 2 minutes. This indicates that the source of small tsunami was close to the George station and travelled a distance of ~ 150 km, indicating a submarine landslide caused by the strike-slip earthquake. The comprehensive analysis shows that the small-scale tsunami was not caused solely by coseismic seafloor deformation from this strike-slip event, but that earthquake-triggered submarine landslide was the primary cause. Hence, the combined effect of two sources leads to the small-scale tsunami.

0. Introduction

At 19:10 on January 28, 2020 (UTC), a large earthquake measuring M_W7.7 (Harvard CMT) struck the Caribbean Sea region (19.421° N, 78.763° W) between Jamaica, the Cayman Islands and Cuba, with a focal depth of 14.8 km. According to reports, the strong shakes were felt across many Caribbean countries, especially in south of Cuba, northwest of Jamaica and the Cayman Islands, and also felt as far away as the United State state of Florida and parts of Mexico (https://www.usatoday.com). Although Caribbean Sea earthquake was large and occurred at an unusually shallow depth, its epicenter was far away from densely populated costal region, so impacts may have been minimized, the loss of human life and destruction of property was minor. According to social media reports (https://www.newsweek.com), the earthquake had a significant impacts on the Cayman Islands, causing a few buildings sustained some damage, cracks in the roads and massive sinkholes in the ground, as well as breaking parts of sewage pipes. Following the earthquake, the Pacific Tsunami Warning Center (PTWC) issued a tsunami warning message (https://tsunami.gov/), forecasting that the earthquake could generate a small tsunami with a maximum wave height of 0.3 to 1 m in parts of Caribbean and adjacent regions such as Cuba, Jamaica, Cayman Islands, Honduras, Mexico and Belize. The tsunami wave observations from coastal sea level gauges in George Town, Cayman Islands indicated that small tsunami waves generated after the earthquake with a 12 cm tsunami wave height recorded on tide gauge in Cayman islands for 11 minutes after the earthquake. In addition, a weak tsunami wave also been measured at the sea level

facility in the port of Morelos in Mexico. Nevertheless, there were no significant impacts on the life of local residents from minor tsunami.

After the M_W7.7 Caribbean Sea earthquake, the USGS and Global Central Moment Tensor Project (GCMT) published the focal mechanism solutions-online, indicating the earthquake was a pure strike-slip shallow event. In general, the megathrust earthquakes are far more likely to generate tsunamis, a sudden vertical deformation of the seafloor due to the dip-slip on the ruptured fault is thought to be the fundamental mechanism of tsunami generation. For the record, megathrust fault slip earthquakes have typically caused tsunamis in recent years, such as the 2004 Indian Ocean tsunami and the 2011 Japan tsunami (Okal & Synolakis, 2008; Fujii et al. 2011). The large strike-slip earthquakes involve motion that is parallel to the fault's strike, where the blocks move on strike-slip fault which are predominantly horizontal and typically considered unfavorable for tsunami generation. However, historical tsunamis associated with major strike-slip earthquakes, such as the 1929 M_W7.2 Grand Banks earthquake, the 1976 M_W7.1 Mindanao, Philippine earthquake, the 1989 M_W6.9 Loma Prieta earthquake, the 1994 M_W7.1 Mindoro, Philippines earthquake, the 1999 M_W7.4 Izmit, Turkey earthquake, the 2010 M_W7.0 Haiti earthquake, and the 2018 M_W7.5 Sulawesi, Indonesia earthquake had been observed resulting to destructive local tsunami (Hasegawa & Kanamori, 1987; Stewart & Cohn, 1979; Ma et al. 1991; Imamura et al. 1995; Altinok et al. 2001; Hornbach et al. 2010; Heidarzadeh et al. 2019). Finally, why do they generate tsunamis? Most of large strike-slip earthquakes triggering submarine landslides and which then produce local tsunamis with significant wave height, but the tectonic deformation from strike-slip faulting should not be overlooked. The large strike-slip fault zones are frequently complex and non-planar geometry, comprising numerous en echelon step-overs, which associated with restraining and releasing bends where topographic uplift and subsidence occur , providing an effective mechanism to induce local tsunamis (Legg & Borrero,2001; Legg et al. 2003). In addition to the previous mentioned factors, deep-water seamounts or other major ocean floor features play a role in tsunami generation (Omira et al. 2016; Pattiaratchi, 2020). So, how did the M_W7.7 strike-slip earthquake in the Caribbean Sea occurred, and what caused the tsunami? Whether tsunamis were triggered by tectonic deformation from M_W7.7 strike-slip earthquake or non-tectonic sources, such as submarine landslides.

The purpose of this study is to understand the seismogenic source of M_W7.7 strike-slip earthquake in the Caribbean Sea and how it generated tsunami. In this context, we gathered the available earthquake data and information, integrating the regional tectonic setting, to reveal earthquake characteristics. Then, we run tsunami simulations using the slip distribution on the finite fault model to see how well the observed and simulated tsunamis waveforms matched. Besides, we performed spectral analysis with wavelet method to shed some lights on the characteristics of the observed tsunami wave. Finally, further research into the mechanisms of the tsunami generated by tectonic or non-tectonic sources is being conducted. This study provides a better understanding of tsunami-generated sources in the Caribbean Sea, and has important implications for the tsunami risk assessment in the Caribbean Sea and surrounding-areas.

1. Regional Tectonic Setting

The 2020 M_W7.7 earthquake struck in the Caribbean Sea between Jamaica, eastern Cuba and Cayman Islands. While the epicenter is located at an active plate boundary between the North American and the Caribbean plate. This plate boundary stretches over 3200 km from northern part of Central America through the Greater Antilles to the northern end of the Lesser Antilles subduction zone, which is a typical left-lateral strike-slip fault zone (Mann et al. 2004). The M_W7.7 earthquake's location and source parameters are highly correlated with the active tectonic structure. According to current GPS measurements, the Caribbean plate is moving east-northeastwards at a rate of about 20 mm/y relative to the North American plate (DeMets et al. 2010). The strike-slip deformation of two tectonic plates, which was accompanied by varying degrees of transpression and transtension (Grindlay et al. 2005), and determined intricate tectonic setting. But what's more complicated is that the northeastern Caribbean plate boundary zone splits into smaller blocks or microplate (van Benthem et al. 2014), they are the Gonâve Microplate, the Hispaniola microplate and the Puerto Rico-Virgin Islands microplate from west to east (Byrne et al. 1985; Rosencrantz and Mann, 1991; Mann et al. 2002).

Sea region

Yellow star denotes the epicenter of 2020 M_W7.7 Caribbean earthquake, filled circles indicate the historical earthquakes from USGS earthquake database. The black beach balls show the focal mechanism of M_W7.7 earthquake given by USGS and GCMT, respectively. The black lines mark the main tectonic-plate faults: MCSC = mid-Cayman spreading center；OFZ = Oriente fault zone；SFZ = Septentrional fault zone, WFZ = Walton fault zone, EPGFZ = Enriquillo-Plaintain Garden fault zone；JRB = Jamaica restraining bend

The M_W7.7 earthquake on January 28,2020, occurred near the boundary of the Gonâve microplate, a small roughly rectangular strip of oceanic crust squeezed between the North American plate and the Caribbean plate. It is bounded to the west by the ultra-slow (15-17 mm/yr) Mid-Cayman Spreading Center (MCSC) (Hayman rt al. 2011) where Cayman Ridge gradually diverges with east-west extension due to the upwelling magma from mantle, and creating the new seafloor and oceanic lithosphere, and the Cayman Trough transforming fault zone and formed a pull-apart basin, its depth over 7000 m, which is the deepest in the Caribbean Sea (Einsele 2000; Lemenkova 2020). The microplate extends eastward until Hispaniola Island or may be diffuse (Benford et al. 2012). To the north bounded by the Septentrional-Oriente fault zone (SOFZ) with main left lateral strike-slip motion at ~10 mm/yr (Symithe et al. 2015), begins northeast of Puerto Rico, extends to west and across the north coast of Hispaniola, runs continuously along the southern end of Cuba, and reaches the Cayman Islands. While the Walton fault zone (WFZ) which extends west along the southern margin of the Cayman Trough, and the Enriquillo–Plantain Garden fault zone (EPGFZ) which extends across the southern part of Hispaniola through the Caribbean to eastern Jamaica, are both major left lateral strike-slip faults, slip along these faults is at ~9 mm/yr (Symithe et al. 2015). The Walton fault zone and Plantain Garden fault zone cannot be traced through Jamaica, where a series of faults known as Jamaica restraining bend exist (JRB) (Benford et al. 2015).

Because of plates interaction leads to strain accumulation and energy release at the plate boundaries, large magnitude earthquakes mainly occurred along the boundaries of the Gonave microplate, where the region has high seismicity. According to the US Geological Survey's historical earthquake database, 25 earthquakes which $M \geq 6.0$ earthquakes have occurred in the Gonâve microplate and its vicinity (14°N-24°N, 84°W-70°W) since the 1900s.. These include two other earthquakes of $M \geq 7.0$, a $M7.0$ Haiti earthquake in 2010, and a $M7.5$ Honduras magnitude in 2018. The $M_W 7.7$ Caribbean earthquake appeared to be the most powerful event in this region. The mainshock appeared to happen in a seismic gap along the Oriente fault, which is the western segment of the Septentrional-Oriente fault zone, and was most likely a characteristic earthquake to fill the seismic gap.

2. Data And Methods

2.1 Earthquake and tsunami observation data

Following the $M_W 7.7$ earthquake in the Caribbean Sea, various earthquake agencies quickly provided the data and information. The USGS (https://earthquake.usgs.gov/earthquakes/eventpage/us60007idc/finite-fault). provides a finite fault model of the $M_W 7.7$ Caribbean earthquake source based on the inverse algorithm (Ji et al., 2002) of teleseismic broadband waveform from the Global Seismic Network (GSN). The spatial distribution of the mainshock and aftershock sequences is depicted in Figure 2 (top panel) and cross-section of slip distribution for $M_W 7.7$ earthquake (bottom panel). The largest slip on the fault plane is over 24 metre. The slip on the Oriente fault zone is mainly strike slip, but there is a significant reverse slip component around the area of the largest slip. Whereas the slip around the Cayman Islands quickly decreases to zero due to the hinder of Cayman Ridge. The Caribbean earthquake ruptured unilaterally to the west of the initial rupture point spanning 180 km along the strike of Oriente fault zone. The rupture was mostly concentrated in the oceanic lithosphere at a relatively shallow depth of 5~25 km. Slip distribution revealed two distinct isolated asperity ruptures: a large slip patch 80~90 km away from the rupture nucleation, and a slightly shallow small patch located at the termination of rupture, where the west end of Oriente fault zone connected with the Cayman Ridge. The spreading centre may obstruct the propagation of a forward rupture.

According to the source characteristics of the $M_W 7.7$ earthquake in the Caribbean Sea, this strong shallow earthquake was predominantly left-lateral strike-slip motion, with a longer surface rupture with concentrated energy release. Moreover, the depth and shape of the seafloor around the earthquake source region are extremely complex, and even minor seafloor uplift or subsidence has the potential to generate tsunamis. Hence,this paper focuses whether the tsunami is caused by vertical coseismic deformation of the seafloor caused by a large strike-slip motion using a tsunami simulation with a finite fault model provided by the USGS.

The General Bathymetric Chart of the Oceans (GEBCO_2020) with 15 arc-sec bathtmetry data was used for tsunami simulation. When the earthquake struck, two coastal tide gauge stations in George Town,

Cayman Islands and Puerto Morelos, Mexico recorded clear tsunami signals. These tide gauges data were acquired from the Sea Level Station Monitoring Facility of IOC (UNESCO) website (http://www.ioc-sealevelmonitoring.org/list.php). To better identify the tsunami, we checked the sea level data for spikes or other potentially abnormal data, and then remove the tidal contribution from the data using a least-square harmonic method from T-tide package with Matlab (Pawlowicz et al. 2002), a band-pass filter is applied to remove high-frequency noise from the tsunami signals. This data pre-processing is only for extracting tsunami signals from raw data, not for spectral analysis. We only use de-tided but unfiltered data for spectral analysis with Matlab wavelet toolboxes. The findings of this study are being considered in order to determine whether the tsunami was primarily caused by the earthquake's coseismic deformation or non-seismic sources.

2.2 Tsunami numerical simulation

The COMCOT (Cornell Multi-grid Coupled Tsunami Model) model's (Liu et al. 1998; Wang and Liu, 2006; Wang 2009) nonlinear shallow water-wave equation was used for numerical tsunami simulations using GEBCO bathymetric data with a resolution of 15 arc-sec.. Tsunami waves (time series) with time step of 0.5 s on coastal tide gauge stations are simulated using static vertical seafloor deformation calculated with Okada's (1992) formula based on the earthquake focal mechanism solutions and finite fault source models provided by USGS. The simulated waveforms are compared to the available tide gauge stations records. The Geoware's (2011) Tsunami Travel Times (TTT) software was used to calculate first-arrival travel time in order to backtrace the potential tsunami sources.

3. What Causes A Micro-tsunami

3.1 Tsunami simulation with finite-fault source model

We only considered the vertical displacement for calculating the initial sea surface height distribution at the tsunami source. The maximum vertical component for coseismic seafloor displacement associated with the M_W7.7 strike-slip earthquake reaches about 1.5 m and appears 80-90 km southwest of the epicenter. The maximum uplift displacement close to the Cayman Islands is only ~0.5 m.

Figure 3b shows the comparison of observed and simulated waveforms of the 2020 Caribbean tsunami. The noticeable sea level fluctuations were recorded on the George Town tide gauge station near the earthquake, ~280 km away from the epicenter; the recorded signals show two distinct phases: within and beyond 30 min of origin time of earthquake. The first phase of the signals shows a leading depression wave followed by a maximum positive amplitude of a short period wave and short duration, a relatively short tsunami travel time (~ 5 min) is measured in George Town station. The subsequent waveform's low-amplitude, long-period, and continuous oscillation characteristics 30 minutes after the earthquake. The numerical simulation predicts that the tsunami waves will arrive at George Town station about 25 minutes after the earthquake; the later observed waveforms' arrival and amplitude are well correlated with the simulated waveforms. The numerical model based on a finite-fault earthquake is unable to fully

reproduce the tsunami amplitude and arrival time recorded on the George Town station. The simulated tsunami wave maximum heights at George Town station are much smaller than those recorded by tide gauge. The Morelos station, located approximately ~860 km from the epicenter of the earthquake, detected weak tsunami wave after the earthquake, the observed and simulated waveforms have similar shapes and oscillation characteristics. As a result of the preceding comparisons, it is sufficient that the M_W7.7 strike-slip earthquake could result in a tsunami caused by coseismic vertical displacement. It is worth noting that the tsunami simulation based on finite fault model is insufficient to support the high-frequency tsunami wave shape and short time arrival recorded on the George station following the early stages of earthquake. Therefore, the characteristic of first phase wave cannot be explained by numerical simulation of earthquake generated tsunami; the early and late tsunami waves recorded on the George Town station may be triggered by two completely different sources and mechanisms. The rapid arrival time of tsunami wave indicates that the possible tsunami-generated source is close to the George Town station. Furthermore, we did not account for the influences in tsunami modeling caused by contributed by limited resolution of the bathymetry and topography data, the uncertainties of the finite fault model and focal mechanism solutions.

3.2 Spectral analysis of sea-level observation waveform

Spectral analysis of tsunami waves may aid in determining the types of tsunami sources. Following the earthquake, we used wavelet method to conduct spectral analysis of sea-level observation on the tide gauge stations (Figure 4). The energy distribution of background noise at George Town station is relatively scattered, and the temporal variability of wave energy is mainly concentrated within 30 minutes after the earthquake; the dominant period with maximum energy is ~ 2 min, which is ~~its~~ shorter than that of the tsunami waves caused by earthquake's source (Higman et al., 2018), Such short-period waves are a hallmark of signature of landslide-induced tsunamis caused by landslides. The later tsunami wave, which occurred ~30 minutes after earthquake, has a larger energy period of ~10 min. The wave energy of the Morelos waves is concentrated in the time range of 60~310 min after the earthquake, indicating that the tsunami wave caused by the earthquake reached the Morelos station. The significant dominant period of tsunami waves is ~30 min around 180 minutes after the mainshock occurrence, which is longer than that of George station.

Within minutes of the earthquake, the George station recorded an unusually short-period tsunami wave. The small tsunami waves could be produced by non-tectonic sources. Bathymetric studies showed that the Cayman Islands areas have complex seafloor relief comprising horsts and graben typical of a spreading center, abnormally deep rift valleys and mountains, steep seafloor slopes (Holcombe et al. 1973; Leroy et al. 2000), these areas are prone to trigger submarine landslides. From numerous videos and images shared on social media (https://www.dominicavibes.dm/news-262161/) showed sinkholes appeared at a number places across the Cayman Islands in the aftermath. What causes sinkholes to happen? Geological surveys indicated that there the Cayman Islands have numerous caves and caverns, both above and below sea level, as a result of carbonates deposited and periodically eroded over the last 30 million years (Jones 1994). When the massive and shallow earthquake struck, the rocks above a cave

or cavity may collapse and form a sinkhole. We suspected that the tremors caused loose sediments or overlying rocks to move along sloping ocean floor resulting submarine landslides or slumps, and that tsunamis were likely generated by associated landslides. It could be the cause of the obvious high frequency large amplitude tsunami waves recorded on the George station in the Cayman Islands after the quake.

3.3 Potential source locations and source length of landslide

According to the reciprocity principle, the tsunami travel time estimated at receiver location starting from source location is similar to that estimated at exchange location. The backward tsunami ray tracing is used to narrow down the scope of possible sources of the high frequency tsunami observed in the Cayman Islands after the 2020 January 28 M_W7.7 Caribbean earthquake. Although the tide gauge measurements are limited in the Cayman Islands, with only one available data, the tsunami ray tracing may help to narrow down the potential tsunami source locations to supplement post-tsunami surveys (Williamson et al. 2019).

The location of George station is regarded as a hypothetical tsunami source, a tsunami propagation time of approximately 8 min is modeled; and the margins of tsunami travel distances after ~8 min define the potential source locations (Figure 6). A short tsunami propagation time in George station indicates the potential source close to the Cayman Islands. The contour of travel time estimation suggested that the possible tsunami source could be located within a 150-kilometer-radius circle centred on the George Town tide gauge. The possible tsunami sources are far away from the region of concentrated energy release of the M_W7.7 earthquake, ruling out the possibility of high frequency tsunami generated by coseismic displacement. In the light of the initial large negative wave in George Town station, we deduced that the possible source region must involve significant seafloor subsidence.

The submarine landslide or slump source dimensions could be estimated based on the dominant period of tsunami equation from Heidarzadeh and Satake (2015):

$$L = \frac{T}{2}\sqrt{gH}$$

In which, L is the length of source, T is the dominant period of tsunami, g is the acceleration of gravity (g = 9.81 m/s^2), H is the average wave depth. The source length of ~5.85 km can be approximately estimated from tsunami dominate period of ~2 min and water depth of 3.5 km at the circle area with 150 km radius with the center at George Town station.

4. Discussion And Conclusions

On January 28, 2020, a M_W7.7 earthquake struct the Caribbean Sea and causing a small tsunami. This study integrates the investigations of regional tectonic setting, earthquake source parameters, tsunami

numerical simulation and spectral analysis to investigate seismogenic fault characterization whether or not the small tsunami is generated by the tectonic source or not.

The GCMT and W-phase moment tensor solutions for the M_W7.7 Caribbean earthquake indicate a strike-slip event, with EW trending consistent with it occurring along the Orient fault zone on the plate boundary between the North American and Caribbean tectonic plates. According to the USGS's finite fault model solutions, the earthquake ruptured predominantly unilaterally in the shallow oceanic lithosphere, starting from the epicenter and extending approximately length of ~180 km westward. The main rupture areas are concentrated around 80~90 km west of epicenter, the maximum slip is ~24 m and there is a small unclear patch distributed at the end of rupture.

The aftershocks for the first two months after the mainshock occurred occurred primarily to the west of the mainshock, particularly near the Cayman Islands, within a much larger zone of 170 km along the Oriente fault. The largest aftershock with a magnitude of 6.1 struck near the end of the rupture zone less than 3 hours, and about 200 kilometers away from the epicenter of mainshock. The *M*w6.1 aftershock's focal mechanism solution (strike = 248° dip = 53° rake = 52°) in Figure 2 indicates that the earthquake occurred a reverse fault characterized by predominantly compressional displacement. The different focal mechanisms suggested that the rupture of a strike-slip earthquake caused by the Oriente fault zone intersecting and terminating against the Cayman Rise can affect the fracture mode of the largest aftershock. The strike-slip displacement moved into the Cayman Rise and causing stress to build up and release in a branch fault from a larger strike-slip fault.

When the simulated tsunami waves were compared to the observed waves, it was clear that the M_W7.7 strike-slip earthquake generated coseismic vertical displacement components that yielded insignificant tsunami. The coseismic rupture of the M_W7.7 strike-slip earthquake also contributed to the observed water level from tide gauge. However, it is clear that the heights of simulated tsunami wave at George Town station are much lower than those recorded on tide gauge station, implying that the small tsunami is not solely generated by tectonic source. The tsunami dominant period is ~2 minutes, according to spectral analysis of the sea-level observation waveform from Gorge Town station, which is much shorter than the period caused by tectonic source. Combining the geological features of Cayman Islands with shared videos and images from social media after the earthquake, the massive earthquake may had triggered submarine landslides or slumps that resultin in a local tsunami.

The possible tsunami source based on backward tsunami ray tracing analysis, could be located within a 150-kilometer-radius circle centred on the George Town tide gauge. It is likely that the intensity shaking observed > VI in the rupture propagation direction from USGS shaking intensity model using the Modified Mercalli Intensity (MMI) scale (https://earthquake.usgs.gov/earthquakes/eventpage/us60007idc/shakemap/intensity), the high shaking intensities resulted in a few significant landslides. The maximum potential source locations are near the Cayman Islands, in the direction of the earthquake's rupture. We could only trace the approximate domain of tsunami source due to the scarcity of available tide gauge sea level data and

bathymetric data. Future works should include multibeam bathymetric sonar, side-scan sonar, seismic sounding profiles and other techniques, to investigate the actual submarine landslide or slump locations.

In the last 400 years, at least 26 tsunami events had occurred in our study area, according to the NCEI/WDS global historical tsunami database, These events have caused large tsunamis with maximum wave heights of up to 3.21 m in Caribbean coastal area. Throughout the entire study area, most tsunamis occurred along the Septentrional-Oriente fault zone and Enriquillo–Plantain Garden fault zone. On June 7, 1692, a devastating earthquake struck Port Royal, Jamaica, causing a landslide in the Royal harbour area and triggering a tsunami with maximum tsunami wave heights over to 1.8 m; 90 percent of the city sank below sea level, about 2,000 people died as a result of the earthquake and the subsequent tsunami (Lander, et al., 2002; Parsons & Geist 2008). The 1842 Cap-Haitian earthquake with a magnitude of 8.1 triggered a destructive tsunami that devastated the northern coast of Haiti and part of Dominican Republic, killing about 300 people. The 2010 Haiti earthquake, a magnitude 7.0, was followed by a deadly local tsunami, which killed at least 7 people According to previous research, the tsunami waves were caused by underwater landslides (Hornbach et al. 2010; Poupardin et al. 2020). There are at least six ~~6~~ landslide-generated tsunamis in the Caribbean Sea near the M_W7.7 earthquake, accounting for 23.1% of all tsunami events. According to the NCEI/WDS global historical tsunami database, only 3% of the global historical tsunami events are associated with submarine landslides. A high proportion of landslide-induced tsunamis is closely related to northern Caribbean's geological structure and tectonic setting.

Since the 1900s, two other earthquakes of $M > 7$ have occurred in the vicinity of the earthquake epicentre,, including a *M*7.0 Haiti earthquake in 2014, and a *M*7.5 Honduras earthquake in 2018 (Figure 7). These earthquakes, along with the M_W7.7 Caribbean earthquake, occurred as the result of strike-slip motion and generated small tsunamis, with a maximum tsunami heights reached 3.21 m, 0.4 m and 0.11 m (Tanioka et al. 2020), respectively. Although small, tsunamis from a large strike-slip earthquake on the northern Caribbean margin are real and have been documented.. There is ~~a~~ enough sufficient evidences to suggest that the Caribbean and neighbouring adjacent regions face a high potential tsunami risk from earthquakes, or submarine landslides. Therefore, tsunami hazard from strike-slip earthquakes or submarine landslides should be considered as part of tsunami vulnerability and risk assessment in the Caribbean and adjacent regions, particularly in densely populated coastal areas.

It is known that tsunami waves propagate at a much slower rate than seismic waves, it is possible to issue tsunami warning information quickly after a major undersea earthquake occurs. However, not all major earthquakes can cause a tsunami, it is difficult to make an accurate forecasting rapidly whether the earthquake will cause tsunami, especially if it is induced by an uncommon tsunamigenic source, such as a direct strike-slip earthquake, or a secondary underwater landslide and so on. In addition, the geometric complexity of the strike-slip fault system triggered multiple rupture segments, resulting in a complex rupture evolution, and the generation of a tsunami, posing a new fresh challenge to tsunami risk assessment and tsunami warning.

Declarations

Acknowledges

We downloaded tide gauge data from the website of Intergovernmental Oceanographic Commission. Historical earthquake catalog and finite fault model solutions are available at the USGS/NEIC website. Earthquake focal mechanism data from GCMT and W-phase moment tensor solution were used in this study. Most figures were plotted by GMT software (Wessel & Smith 1998), part of figures were drawn using Matlab packages.

References

Altinok Y, Tinti S, Alpar B, Yalciner AC, Ersoy Ş, Bortolucci E, & Armigliato A (2001) The tsunami of August 17, 1999 in Izmit bay, Turkey. Natural Hazards 24(2), 133–146.

Benford B, DeMets C, Tikoff B, Williams P, Brown L, & Wiggins-Grandison M (2012) Seismic hazard along the southern boundary of the Gônave microplate: block modelling of GPS velocities from Jamaica and nearby islands, northern Caribbean. Geophysical Journal International 190(1), 59–74.

Benford B, Tikoff B, & DeMets C (2015) Interaction of reactivated faults within a restraining bend: Neotectonic deformation of southwest Jamaica. Lithosphere 7(1), 21–39.

Byrne DB, Suarez G, & McCann WR (1985) Muertos Trough subduction-Microplate tectonics in the northern Caribbean?. Nature 317(6036), 420–421.

DeMets C, Gordon RG, & Argus DF (2010) Geologically current plate motions. Geophysical Journal International 181(1), 1–80.

Einsele G (2000) Sedimentary basins: evolution, facies, and sediment budget. Springer Science & Business Media.

Fujii ., Satake K, Sakai SI, Shinohara M, & Kanazawa T (2011) Tsunami source of the 2011 off the Pacific coast of Tohoku Earthquake. Earth, planets and space 63(7), 815–820.

Geoware (2011), The Tsunami Travel Times (TTT). Available at http://www.geoware-online.com/tsunami.html.

Grindlay NR, Hearne M, & Mann P (2005) High risk of tsunami in the northern Caribbean. Eos, Transactions American Geophysical Union 86(12), 121–126.

Hasegawa HS, Kanamori H (1987) Source mechanism of the magnitude 7.2 Grand Banks earthquake of November 1929: Double couple or submarine landslide?. Bulletin of the seismological Society of America 77(6), 1984–2004.

Hayman NW, Grindlay NR, Perfit MR, Mann P, Leroy S, & de Lépinay BM (2011) Oceanic core complex development at the ultraslow spreading Mid-Cayman Spreading Center. Geochemistry, Geophysics,

Geosystems 12(3).

Heidarzadeh M, & Satake K (2015) New insights into the source of the Makran tsunami of 27 November 1945 from tsunami waveforms and coastal deformation data. Pure and Applied Geophysics 172(3), 621–640.

Heidarzadeh M, Muhari A, & Wijanarto AB (2019) Insights on the source of the 28 September 2018 Sulawesi tsunami, Indonesia based on spectral analyses and numerical simulations. Pure and Applied Geophysics 176(1), 25–43.

Higman B, Shugar DH, Stark CP, Ekström G, Koppes MN, Lynett P, ... & Loso M (2018). The 2015 landslide and tsunami in Taan Fiord, Alaska. Scientific Reports 8(1), 1–12.

Holcombe TL, Vogt PR, Matthews JE, & Murchison RR (1973) Evidence for sea-floor spreading in the Cayman Trough. Earth and Planetary Science Letters 20(3), 357–371.

Hornbach MJ, Braudy N, Briggs RW, Cormier MH, Davis MB, Diebold JB, ... & Templeton J (2010) High tsunami frequency as a result of combined strike-slip faulting and coastal landslides. Nature Geoscience 3(11), 783–788.

Imamura F, Synolakis CE, Gica E, Titov V, Listanco E, & Lee HJ (1995) Field survey of the 1994 Mindoro Island, Philippines tsunami. Pure and applied geophysics 144(3), 875–890.

Ji C, Wald DJ, & Helmberger DV (2002) Source description of the 1999 Hector Mine, California, earthquake, part I: Wavelet domain inversion theory and resolution analysis. Bulletin of the Seismological Society of America 92(4), 1192–1207.

Jones B (1994) Geology of the Cayman Islands. In The Cayman Islands (pp. 13–49). Springer, Dordrecht.

Lander JF, Whiteside L, & Lockridge PA (2002) A brief history of tsunamis in the Caribbean Sea. Science of Tsunami Hazards, 20(2), 57–94.

Legg MR, & Borrero JC (2001) Tsunami potential of major restraining bends along submarine strike-slip faults. In Proceedings of the international tsunami symposium (pp. 331–342).

Legg MR, Borrero JC, Synolakis CE (2003) Tsunami hazards from strike-slip earthquakes. In AGU Fall Meeting Abstracts (Vol. 2003, pp. OS21D–06).

Lemenkova, P (2020) Geomorphology of the Puerto Rico Trench and Cayman Trough in the Context of the Geological Evolution of the Caribbean Sea. Annales Universitatis Mariae Curie-Sklodowska, sectio B–Geographia, Geologia, Mineralogia et Petrographia, 75, 115–141.

Leroy S, Mauffret A, Patriat P, & Mercier de Lépinay B (2000) An alternative interpretation of the Cayman trough evolution from a reidentification of magnetic anomalies. Geophysical Journal International 141(3),

539–557.

Liu PL-F, Woo SB, Cho Y (1998) Computer designed for Tsunami Propagation and Inundation. Cornell University, Sponsored by the National Science Foundation, 104.

Ma K-F, Satake K, & Kanamori H (1991) The origin of the tsunami excited by the 1989 Loma Prieta Earthquake -Faulting or slumping? Geophysical Research Letters 18(4), 637–640.

Mann P, Calais E, & Huerfano V (2004) Earthquake shakes a big bend region of north America-Caribbean boundary zone. EOS Transactions American Geophysical Union 85(8), 77–83.

Mann P, Calais E, Ruegg JC, DeMets C, Jansma PE, & Mattioli GS (2002) Oblique collision in the northeastern Caribbean from GPS measurements and geological observations. Tectonics 21(6), 7–1.

National Geophysical Data Center / World Data Service: NCEI/WDS Global Historical Tsunami Database. NOAA National Centers for Environmental Information. doi:10.7289/V5PN93H7 [access August 2020]

Okada, Y (1992) Internal deformation due to shear and tensile faults in a half-space. Bulletin of the Seismological Society of America 82: 1018–1040.

Okal EA, Synolakis CE (2008) Far-field tsunami hazard from mega-thrust earthquakes in the Indian Ocean. Geophysical journal international 172(3): 995–1015.

Omira R, Ramalho I, Terrinha P, Baptista MA, Batista L, & Zitellini N (2016). Deep-water seamounts, a potential source of tsunami generated by landslides? The Hirondelle Seamount, NE Atlantic. Marine Geology 379, 267–280.

Parsons T, & Geist EL (2008) Tsunami probability in the Caribbean region. In Tsunami Science Four Years after the 2004 Indian Ocean Tsunami (pp. 2089–2116). Birkhäuser Basel.

Pattiaratchi C (2020) Influence of Ocean Topography on Tsunami Propagation in Western Australia. Journal of Marine Science and Engineering 8(9), 629.

Pawlowicz R, Beardsley B, & Lentz S (2002) Classical tidal harmonic analysis including error estimates in MATLAB using T_TIDE. Computers & Geosciences 28(8), 929–937.

Poupardin A, Calais E, Heinrich P, Hébert H, Rodriguez M, Leroy S, ... & Douilly R (2020) Deep submarine landslide contribution to the 2010 Haiti earthquake tsunami. Natural Hazards and Earth System Sciences, 20(7), 2055–2065.

Rosencrantz E, & Mann P (1991) SeaMARC II mapping of transform faults in the Cayman Trough, Caribbean Sea. Geology 19(7), 690–693.

Stewart GS, & Cohn SN (1979) The 1976 August 16, Mindanao, Philippine earthquake (Ms = 7.8) - evidence for a subduction zone south of Mindanao. Geophysical Journal International 57(1), 51–65.

Symithe S, Calais E, De Chabalier JB, Robertson R, & Higgins M (2015) Current block motions and strain accumulation on active faults in the Caribbean. Journal of Geophysical Research: Solid Earth 120(5), 3748–3774.

Tanioka Y, Cabrera AG, Arguello GJ, & Yamanaka Y (2020) Tsunami hazard in the Caribbean coast of Honduras due to large earthquakes occurred along the Cayman Trough at the northwest boundary of Caribbean plate. Coastal Engineering Journal 62(3), 405–412.

van Benthem S, Govers R, & Wortel R (2014) What drives microplate motion and deformation in the northeastern Caribbean plate boundary region?. Tectonics 33(5), 850–873.

Wang XM (2009) Technical document for COMCOT v.1.7. Institute of Geological and Nuclear Science, New Zealand.

Wang XM, Liu PL-F (2006) An analysis of 2004 Sumatra earthquake fault plane mechanism and Indian Ocean tsunami. J Hydraul Res 44(2):147–154.

Wessel, P., & Smith, W. H. (1998). New, improved version of Generic Mapping Tools released. Eos, Transactions American Geophysical Union, 79(47), 579–579.

Williamson A, Melgar D, Xu X, & Milliner C (2019) Coseismic or Landslide? The source of the 2018 Palu Tsunami.

Figures

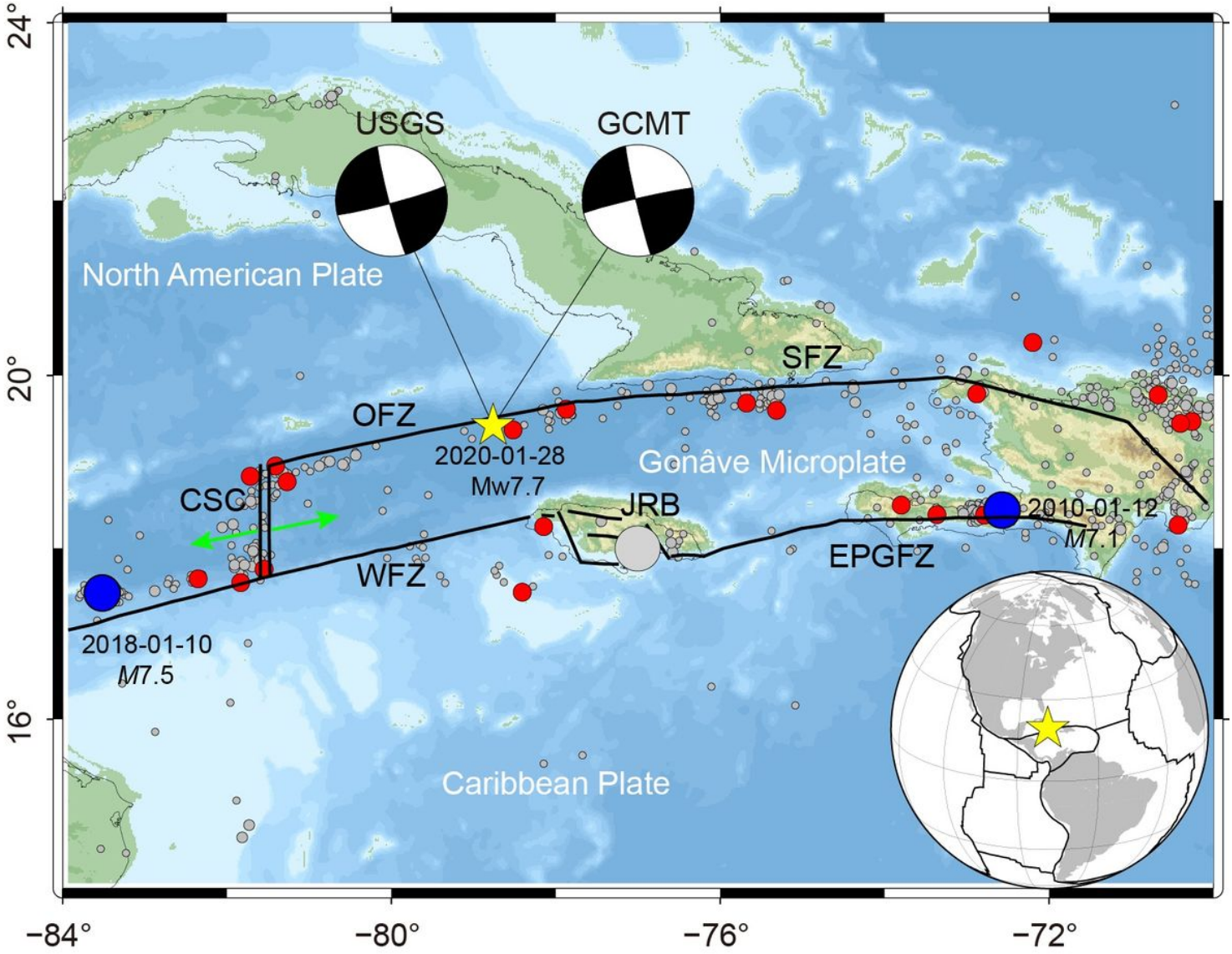

Figure 1

The regional tectonic setting and historical earthquakes in the Caribbean Sea region Yellow star denotes the epicenter of 2020 MW7.7 Caribbean earthquake, filled circles indicate the historical earthquakes from USGS earthquake database. The black beach balls show the focal mechanism of MW7.7 earthquake given by USGS and GCMT, respectively. The black lines mark the main tectonic-plate faults: MCSC = mid-Cayman spreading center；OFZ = Oriente fault zone；SFZ = Septentrional fault zone, WFZ = Walton fault zone, EPGFZ = Enriquillo-Plaintain Garden fault zone；JRB = Jamaica restraining bend

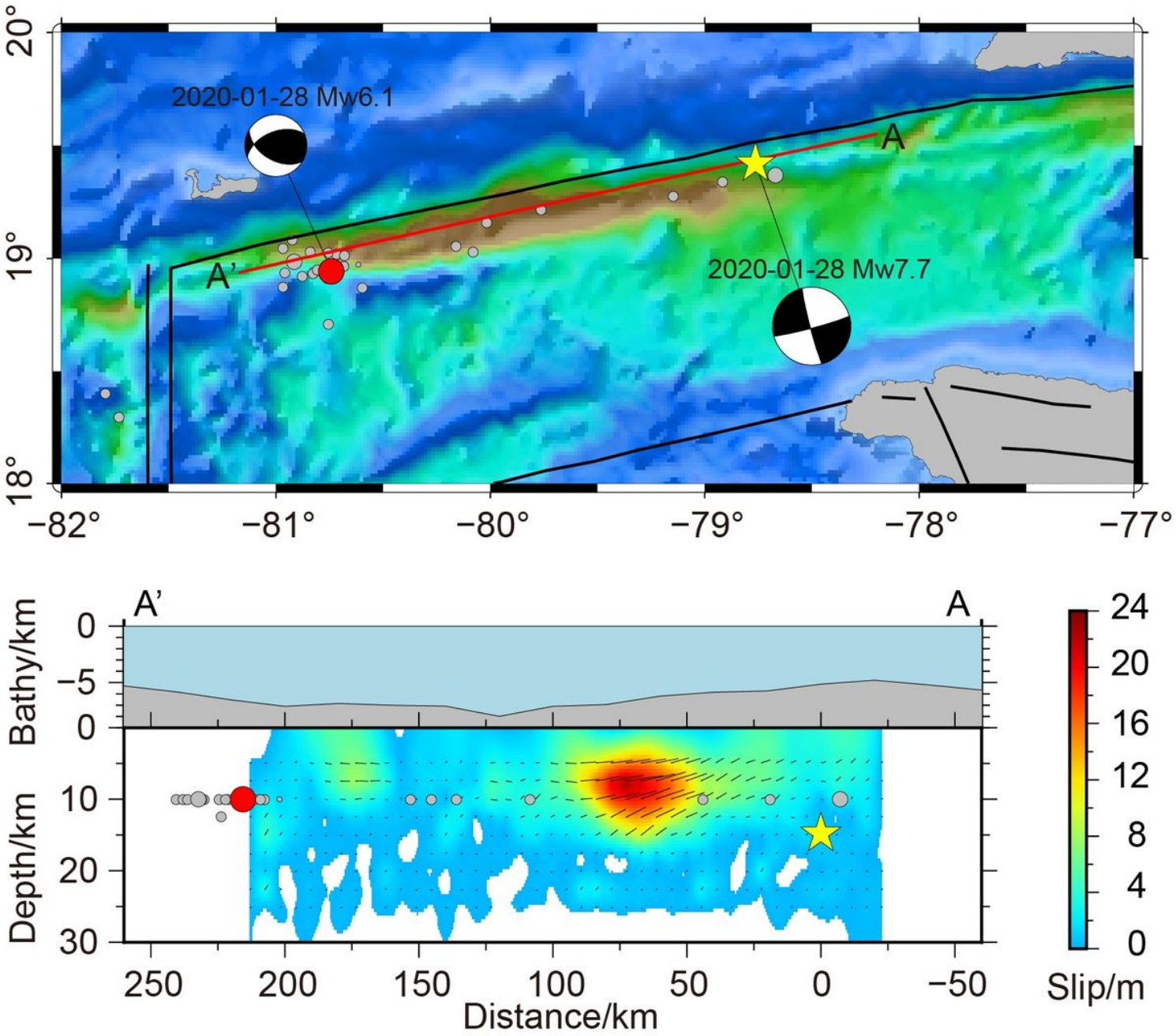

Figure 2

Map view of mainshock and aftershocks and cross-section of slip distribution of MW7.7 Caribbean earthquake Black line denotes the main faults, mainshock and aftershock are plotted by a yellow star and filled circles, separately, red solid circle shows the largest aftershock (MW = 6.1) following the mainshock. The color bar shows the slip amplitude and black arrows indicate the slip direction

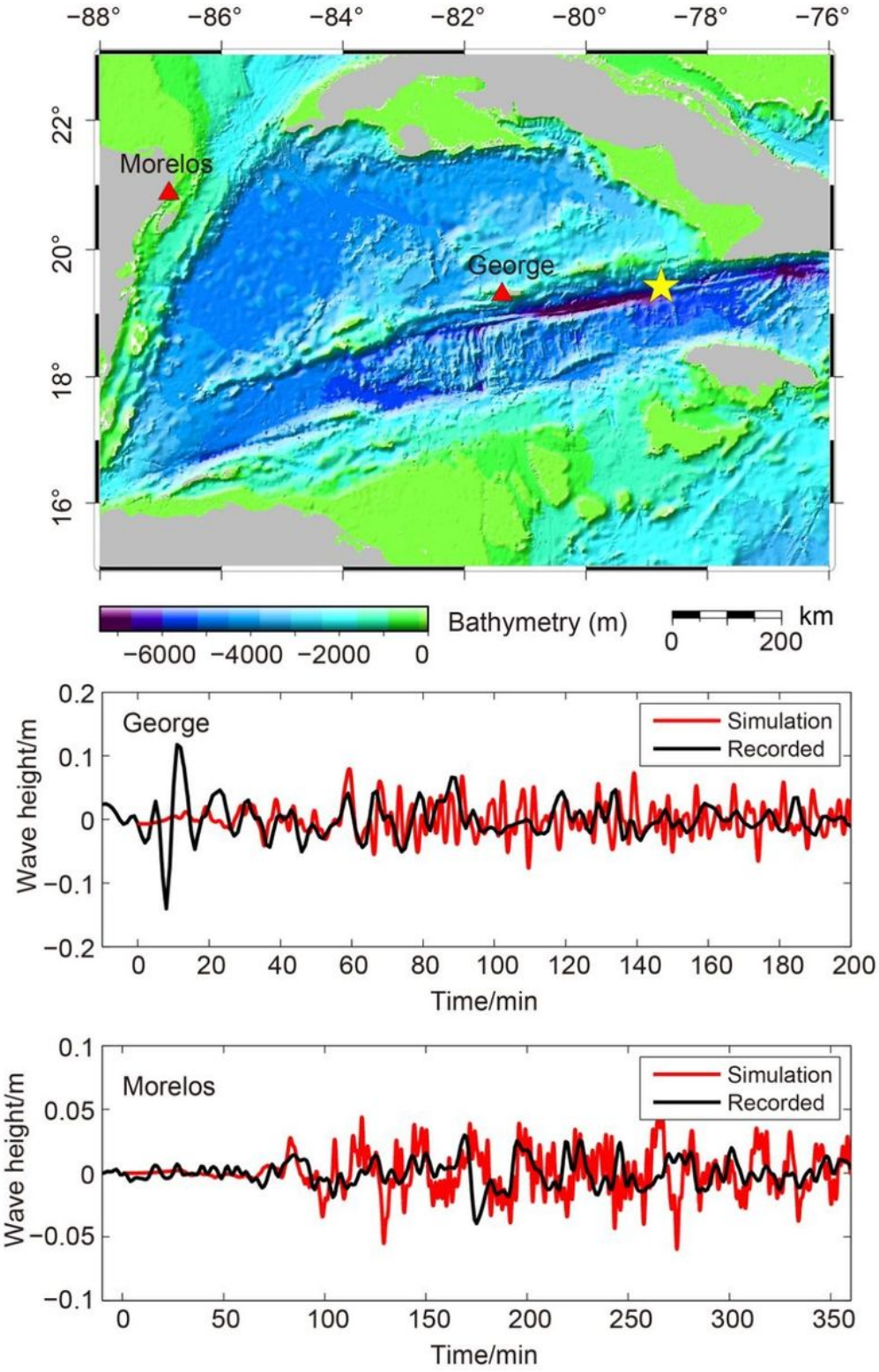

Figure 3

Results of tsunami simulations using finite-fault slip distributions from USGS (a) The bathymetry data used for tsunami modeling, red triangles show the location of the coastal tide gauges, yellow star represents the epicenter of the MW7.7 Caribbean earthquake. (b) and (c) show the comparisons between simulated (red line) and recorded (black line) tsunami waves, the letters on the left top of panel indicate the code of tide gauge station.

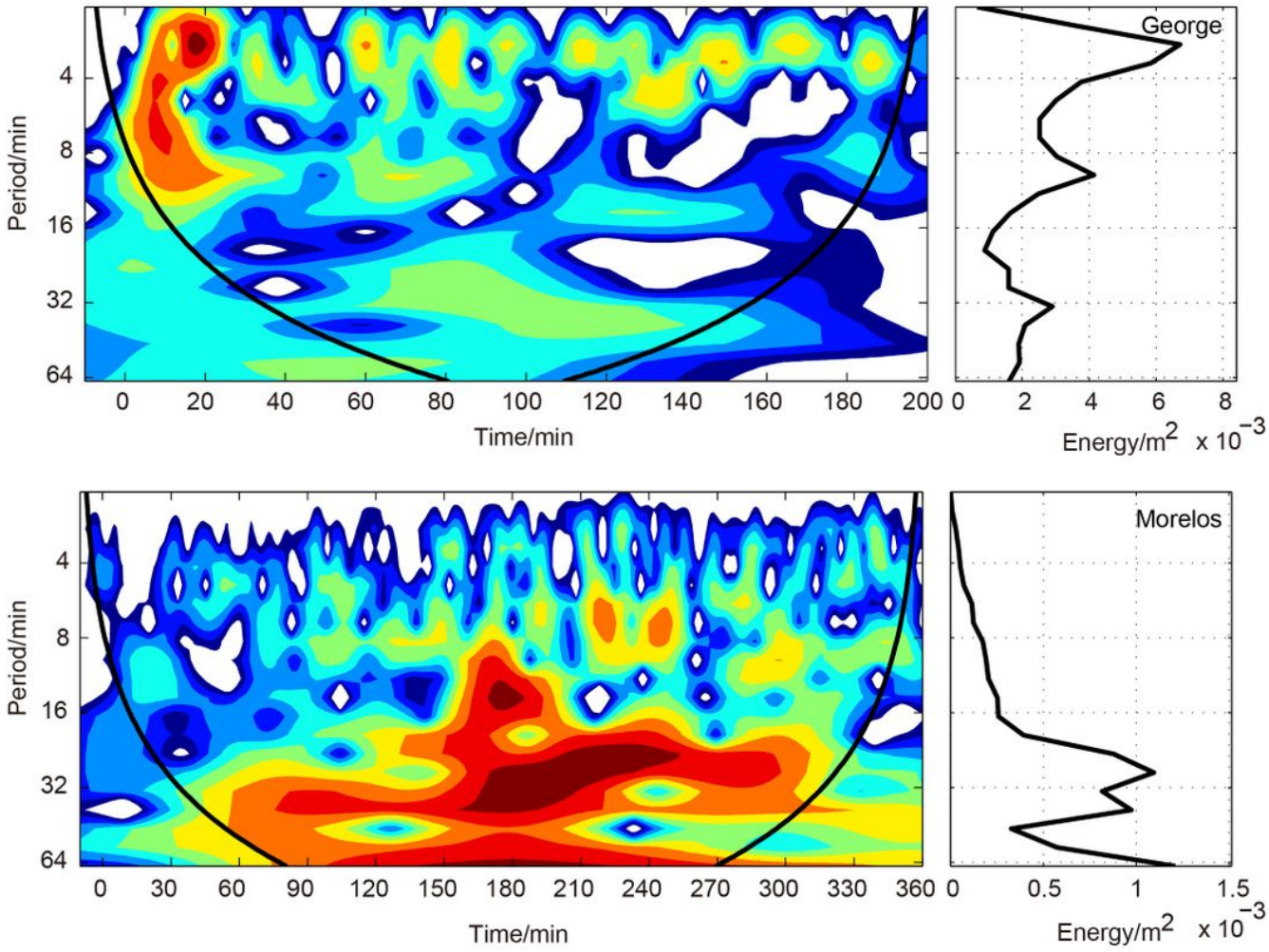

Figure 4

The spectral analysis of sea-level observations on George Town and Puerto Morelos station The thick line on the left-plot describes the 95% confidence interval of wavelet power

Figure 5

Sinkholes appeared on the Cayman Islands after the massive earthquake, the images come from social media website (https://www.dominicavibes.dm/news-262161/)

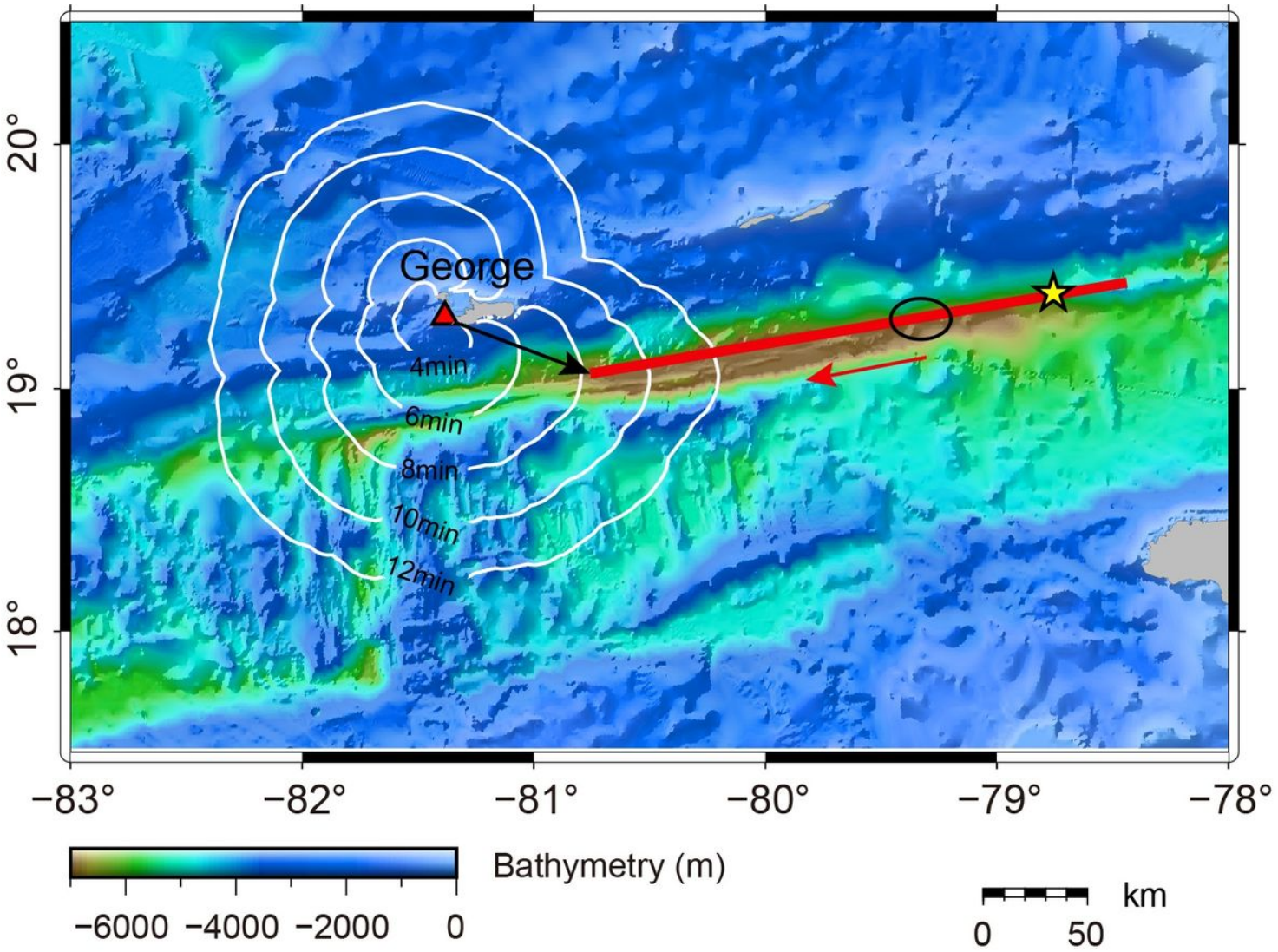

Figure 6

Tsunami travel time rays tracing in the locations of George Town station using GEBCO_2020 bathymetric data Red triangle denotes the location of George Town station as a hypothetical tsunami source for tsunami travel time estimation (white line), the possible location of tsunami source is indicated by black arrow. Red thick line and arrow show the length and propagation direction of rupture of MW7.7 Caribbean earthquake, respectively. Black ellipse remarks the location of concentrated energy release, epicenter of mainshock is drawn as yellow star

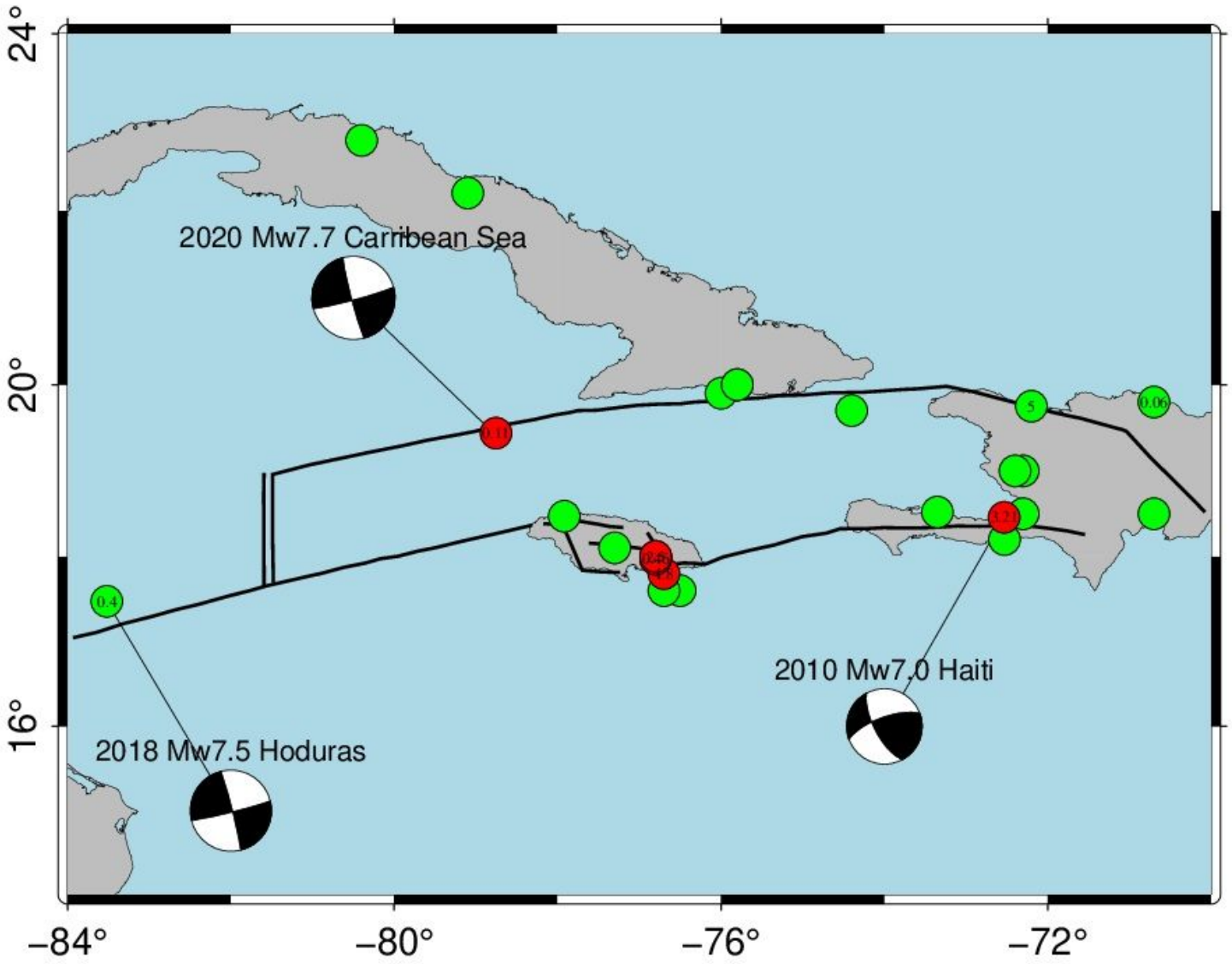

Figure 7

Historical tsunamis occurred in our study area in the past 400 years. Black solid line shows the main boundary fault in this study area, colored circles indicate the distribution of historical tsunami sources, red (earthquake-generated tsunami)and green (landslide-induced tsunami) color are the types of tsunami sources, the number on the circles represents the maximum tsunami heights. The historical tsunami data are from the NCEI/WDS global historical tsunami database, the focal mechanism solutions are from the GCMT